ARTICLE

Vortex-induced Vibration of Elastically Connected Multiple Circular Cylinders in a Side-by-side Arrangement in Steady Flow

Kalyani Kaja   Ming Zhao[*]

School of Computing, Engineering and Mathematics, Western Sydney University, Locked Bag 1797, Penrith, NSW 2751, Australia

ARTICLE INFO	ABSTRACT
	Vortex-induced vibration (VIV) of multiple circular cylinders elastically connected together in a side-by-side arrangement subject to steady flow is investigated numerically at a low Reynolds number of 150 and a mass ratio of 2. Simulations are conducted for two-, five- and ten-cylinder systems over a wide range of reduced velocities. The aim of the study is to identify the high-amplitude response range of the reduced velocity for the multiple degree of freedom vibration system and identify the difference between the responses of the single- and multiple-degree-of-freedom vibrations. Unlike the single cylinder case, distinct lock-in between the response frequency and any of the structural natural frequencies in a wide range of reduced velocity is not observed in the multiple-cylinder cases. Instead, the response frequency increases continuously with increasing reduced velocity. High response amplitudes are found when the response frequency is between the first and the highest modal frequencies. In a multiple-cylinder system, the single-mode response, where the vibration is dominated by one mode, can be only found in low reduced velocity range. In the single-mode branch, the dominance of a single mode shape in the response can be clearly identified except at the boundary reduced velocity between two modes. The maximum response amplitude occurs in the multiple-mode response and interaction between the vortices in the wake of the cylinders is strong when the response amplitudes are high.

1. Introduction

Vortex-induced vibrations (VIV) of cylindrical structures are of engineering significance because excessive vibrations may lead to malfunction and even structural failure. When an elastically mounted cylinder is placed in a free stream, synchronization (or the lock-in) occurs in a range of reduced velocity [1-4]. When lock-in occurs, the vortex shedding frequency is the same as the vibration frequency of the cylinder, instead of fol-

lowing the Strouhal law [5]. When an elastically mounted cylinder vibrates in the cross-flow direction in a fluid flow at low mass ratios, the range of the reduced velocity is divided into three branches: initial, upper and lower branches [6,7]. Jauvtis and Williamson [8] found a super upper branch for two-degree-of-freedom (2DOF) VIV of a circular cylinder in both the in-line and cross-flow directions at low mass ratios. The vibration of a circular cylinder in steady flow close to a plane boundary was also investigated due to its engineering importance [9-12]. It was found that

DOI: https://doi.org/10.30564/hsme.v2i1.1504

1

the plane boundary has significant effects on the vibration of the cylinder.

Numerical studies of VIV have been mostly conducted through two-dimensional simulations by solving either the 2D Navier-Stokes (NS) equations or the 2D Reynolds-Averaged Navier-Stokes equations (RANS). The numerical models based on the NS equations have provided satisfactory numerical solutions for VIV of a circular cylinder at low Reynolds numbers in the laminar flow regime [13-17]. The numerical models based on the RANS equations were found to provide satisfactory solutions of VIV of cylinders at higher Reynolds numbers in the subcritical flow regime [18,19].

The research of flow past multiple cylinders has been mainly focused on flow past two cylinders in different arrangements. The biased flow regime when the gap between the cylinders is small was found in many studies of flow past two cylinders in a side-by-side arrangement [20,21]. Numerical studies of flow past two cylinders in side-by-side arrangement have also been conducted and the numerical results of the biased flow were found to agree well with the experimental data [22,23]. Recently, some studies of VIV of two or four cylinders have also been conducted both experimentally and numerically. Huera-Huarte and Gharib [24] conducted laboratory experiments of VIV of two side-by-side flexible cylinders at low mass ratios. It was found that the motions of the two cylinders are not synchronized if the centre-to-centre distance between the two cylinders is greater than 3.5 diameters. Wang et al. [25] focused their study of VIV of two side-by-side cylinders on the influence of the turbulence and found that the free-stream turbulence enhances the vortex-induced force and thus restores the large amplitude vibration associated with the lock-in resonance. Assi et al. [26] conducted experiments of VIV of an elastically mounted cylinder in the wake of a fixed identical cylinder and found that when the gap between the two cylinders is between 3 to 5.6 diameters, the vibration is in a galloping-like pattern. Kim et al. [27] studied VIV of two elastically mounted cylinders in a tandem arrangement and found five response regimes, depending on the distance between the two cylinders. Numerical studies of VIV of two cylinders have also been conducted recently [28-34], where the two cylinders were either in side-by-side, tandem or staggered arrangement.

Multiple cylinders are sometimes used in the fluid engineering, such as the multiple mooring cable in the offshore engineering or multiple heat exchanger tubes. If multiple-cylinders are elastically connected together, the system is a multiple-degree-of-freedom system with multiple natural frequencies. So far, little attention has been paid on VIV of elastically connected multiple cyl-

inder systems. Lock-in regime of the reduced velocity of elastically connected cylinders in fluid flow is expected to be wider than that of a single cylinder. Which natural frequencies the cylinders vibration locks onto is expected to depend on the reduced velocity.

In this study, VIV of elastically connected multiple circular cylinders in a side-by-side arrangement in steady flow is simulated numerically at a low Reynolds number of 150 and a low mass ratio of 2. The focus of the study is to investigate the response and lock-in behaviors of multi-degree-of-freedom (MDOF) systems. Since the flow is expected to be two-dimensional at Re=150, two-dimensional Navier-Stokes equations are solved using the Petrov-Galerkin finite element method for simulating the flow and the equation of the motion of the cylinders is solved using the fourth-order Runge–Kutta method for predicting the response of the cylinders.

2. Numerical Method

Flow induced vibration of elastically connected circular cylinders as shown in Figure 1 is simulated numerically. The cylinders are allowed to vibrate in the cross-flow direction only. It is assumed that diameter and mass of the cylinders are all identical. The initial distance between two adjacent cylinder centres is fixed at a constant of *L*=3*D* with *D* being the diameter of the cylinders. The differential equation of motion governing the vibration of the cylinders can be written as

$$\mathbf{M}\ddot{\mathbf{Y}} + \mathbf{C}\dot{\mathbf{Y}} + \mathbf{K}\mathbf{Y} = \mathbf{F}_{\mathrm{y}}, \qquad (1)$$

where M, C and K are the symmetric mass, damping and stiffness matrices, respectively. The displacement vector Y contains the displacements of the cylinders in the cross-flow direction and is given by $\mathbf{Y} = \{Y_1, Y_2, \ldots Y_N\}^T$, F_y is the corresponding vector of the forces on the cylinders, and N is the number of cylinders considered. The natural frequencies and the mode vectors of the system can be obtained by calculating the eigenvalues and the eigenvectors of the stiffness matrix. The solution of Eq. (1) can be expressed in the form

$$\mathbf{Y}(t) = \mathbf{\Phi}\mathbf{Y}^*(t), \qquad (2)$$

where $\mathbf{\Phi} = \{\mathbf{\Phi}_1, \mathbf{\Phi}_2, \cdots, \mathbf{\Phi}_N\}$ is the modal matrix of the system, $\mathbf{\Phi}_k$ stands for the kth-mode vector, and $\mathbf{Y}^*(t)$ is a column vector of generalized (modal) coordinates that are to be determined. The modal matrix $\mathbf{\Phi}$ satisfies $\mathbf{\Phi}^T\mathbf{M}\mathbf{\Phi} = \mathbf{I}$ where $\mathbf{I}$ is the unit matrix. The amplitude of $\mathbf{Y}^*(t)$ is comprised of the response component of each mode. Substituting Eq. (2) into Eq. (1) yields

$$\ddot{\mathbf{Y}}^* + \mathbf{C}^* \dot{\mathbf{Y}}^* + \mathbf{K}^* \mathbf{Y}^* = \mathbf{F}_y^*, \qquad (3)$$

where $\mathbf{C}^* = \mathbf{\Phi}^T \mathbf{C} \mathbf{\Phi}$, $\mathbf{K}^* = \mathbf{\Phi}^T \mathbf{K} \mathbf{\Phi}$ and $\mathbf{F}_y^* = \mathbf{\Phi}^T \mathbf{F}_y$. The matrix $\mathbf{K}^*$ is a diagonal matrix and zero damping is considered in this study. The above modal transformation method enables the vibration problem to be solved without solving the matrix equations. This modal transformation method also enables to understand the contributions of different modes in the vibration straightforwardly. Eq. (3) is solved by using the fourth-order Runge–Kutta method in this study.
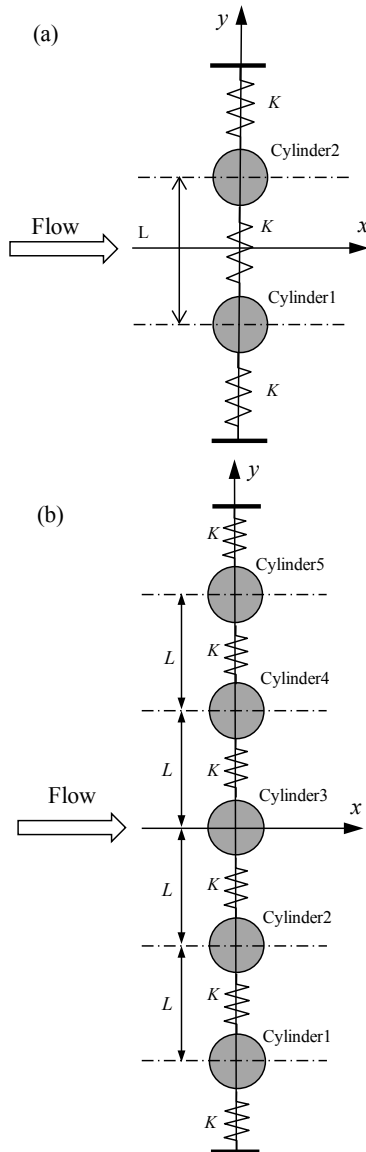

Figure 1. Sketch of elastically connected side-by-side cylinders in fluid flow (a) two cylinder (b) multiple cylinders

The governing equations for simulating the laminar flow are the unsteady two-dimensional incompressible Navier-Stokes equations. In this study, the Arbitrary Lagrangian Eulerian (ALE) scheme is applied to deal with the moving boundaries of the cylinders. Lagrangian method, Eulerian method and ALE method are three methods for tracking the moving boundaries of the fluid domain in numerical simulations. The computational mesh in do not move in the Eulerian method and move at velocities same as the velocity of the fluid particles in the Lagrangian method. The main drawback of the Lagrangian method is that it will face severe problems when deal with strong distortions of the computational mesh and the main disadvantage of the Euler method is that it is difficult to accurately capture the interfaces between the fluid and structure [32]. In the ALE method, the computational domain is moved according to an artificial domain velocity, which ensures that the interfaces can be clearly defined and the computational domain is not distorted strongly [32]. In the ALE scheme, the nodes of the computational mesh are allowed to move at velocities different from the fluid velocities. The incompressible Navier-Stokes equations in the ALE scheme can be expressed as

$$\frac{\partial u_i}{\partial x_i} = 0, \qquad (4)$$

$$\frac{\partial u_i}{\partial t} + \left(u_j - \hat{u}_j \right) \frac{\partial u_i}{\partial x_j} = -\frac{1}{\rho} \frac{\partial p}{\partial x_i} + \nu \frac{\partial^2 u_i}{\partial x_j^2}, \qquad (5)$$

where $x_1 = x$ and $x_2 = y$ are the Cartesian coordinates in the in-line and transverse directions of the flow, respectively, u_i is the fluid velocity component in the x_i-direction, p is the pressure, $\hat{u}_i$ is the velocity of the mesh movement, ρ is the fluid density and ν is the kinematic viscosity. For uniform flow past cylinders, the inlet boundary conditions are set as $u_1 = U$ and $u_2 = 0$. At the outlet boundary, the pressure is set to be zero and the gradient of the velocity components in the streamwise direction is zero [33]. At the cylinder surfaces, non-slip boundary condition is imposed, *i.e.* the fluid velocity is the same as the vibration velocity of the cylinders. After each computational time step, the boundary of the computational domain changes because of the displacements of the cylinders. The positions of finite element nodes are moved accordingly by solving the modified Laplace equation [12]

$$\nabla \cdot \left(\gamma \nabla S_y \right) = 0 \qquad (6)$$

where, S_y represents the displacement of the nodal points in the *y*-direction, γ is a parameter that controls the

mesh deformation. In order to avoid excessive deformation of the near-wall elements, the parameter γ in a finite element is set to be $\gamma = 1/A$, with A being the area of the element. The displacement of the mesh nodes is the same as the displacement of the cylinder on the cylinder surface and zero on other boundaries. By giving the displacements at all the boundaries, Eq. (6) is solved by the Galerkin FEM.

3. Numerical Results

The study is focused on the influence of the interference among multiple circular cylinders in a side-by-side arrangement on the response amplitudes and frequencies. Figure 1 shows a sketch of the arrangement of the cylinder system. The cylinders are numbered by cylinder 1 to cylinder N, respectively, where N is the total number of the cylinders. The springs that connect the cylinders have the same elastic coefficient of K. The cylinders are identical to each other and they have the same mass ratio of 2. The structural damping factor of the whole system is assumed to be 0 in all the simulations. The initial center-to-center distance between any two adjacent cylinders is 3D. In the review paper of flow past two cylinders in a side-by-side arrangement, Sumner [34] concluded that two parallel vortex streets occur in the wake of the two cylinders due to the weak wake interference if the gap between the two cylinders is greater than 1D. Because this study is focused on the effects of the multiple-degree-of-freedom on the response regime of the reduced velocity, the initial gap between two adjacent cylinders is chosen to be sufficiently large. The Reynolds number based on the cylinder diameter is fixed to be 150. Simulations are carried for two-cylinder, five-cylinder and ten-cylinder systems. The reduced velocity is defined based on the first mode natural frequency as $V_r = U/(f_{n1}D)$, where f_{n1} is the first-mode structural natural frequency of the cylinders and U is the free-stream velocity. The responses of different systems are addressed separately in the following discussion.

Zhao et al. [35] found that the wake flow in the wake of elastically mounted cylinder remains two-dimensional until the Reynolds number is 250 when the reduced velocity is 6, where the response amplitude reaches its maximum. To demonstrate that the flow is two dimensional for a Reynolds number of 150, some three-dimensional simulations of VIV of the five-cylinder system are performed for a reduced velocity of 7, which is in the middle of the lock-in range. The numerical method used for the three-dimensional simulation is the same as the one in Zhao et al. [35]. The computational mesh on the cross-sectional plane is the same as used in this study. The length of the cylinders is 6.4 diameters and totally 64 layers of elements are dis-

tributed along the axial direction of the cylinders. The total element number is about 2.2 million. 16 CPUs are used for the parallel calculations. Three-dimensional numerical simulations are performed for a non-dimensional time of $tf_{n1}=19$ and Figure 3 (a) and (c) shows the time histories of cylinders 1 and 5. The symmetric vibration develops to asymmetric vibration after $tf_{n1}=6$ for both Reynolds numbers.

The three-dimensional vortex shedding flow structure can be presented by the iso-surface of the second negative eigenvalue of the tensor $\mathbf{\Psi}^2 + \mathbf{\Omega}^2$, where $\mathbf{\Psi}$ and $\mathbf{\Omega}$ are the symmetric and the anti-symmetric parts of the velocity-gradient tensor, respectively [36]. The nondimensional second eigenvalue is defined as $\lambda_2 = \lambda_2'/(U/D)^2$, where λ_2' is dimensional eigenvalue. The iso-surfaces of $\lambda_2 = -1$ for Re=250 and 300 at $tf_{n1}=18.5$ are shown in Figure 3 (b) and (d), respectively. It can be clearly seen that the flow is still two-dimensional when Re=250 and becomes three-dimensional when Re=300. It is interesting to see that the three-dimensional flow is mainly in the wake of the middle cylinder, where the wake flow is dominated by streamwise vortices. The three-dimensionality of the flow can be quantified by enstrophies [37]. The primary enstrophy ε_z, the secondary ε_{xy} and the total enstrophy ε are defined as $\varepsilon_z = \int_\Omega \omega_z^2 \, \mathrm{d}\Omega$,

$$\varepsilon_{xy} = \int_\Omega (\omega_x^2 + \omega_y^2)\,\mathrm{d}\Omega, \quad \varepsilon = \int_\Omega (\omega_x^2 + \omega_y^2 + \omega_z^2)\,\mathrm{d}\Omega$$

, respectively, where Ω stands for the whole fluid volume. The flow is three-dimensional if the secondary enstrophy is strong and two-dimensional if the secondary enstrophy is zero. For the five-cylinder system, the nondimensional total enstrophies for Re=250 and 300 are $\varepsilon/(U/D)^2 = 2.98 \times 10^5$ and 4.14×10^5, respectively, and the nondimensional secondary enstrophies for Re=250 and 300 are $\varepsilon_{xy}/(U/D)^2 = 3.13 \times 10^{-1}$ and 1.60×10^4, respectively. The negligibly small secondary enstrophy for Re=250 demonstrates that the flow is still two-dimensional. For Re=300, the secondary enstrophy still takes very small percentage in the total enstrophy, mainly because the three-dimensionality is strong only in the wake of the middle cylinder as shown in Figure 3 (d). If the flow is two-dimensional at Re=250, it is expected that the flow should be also two-dimensional when Re<250.

3.1 Two-cylinder System

Simulations are carried out for the reduced velocities ranging from 1 to 30 with an interval of 1 for the two-cylinder system. The ratio of the first- to second-mode natural frequencies is $f_{n2}/f_{n1}=1.732$. A rectangular computational domain with a length in the flow direction of 60D is

used. The width of the computational domain (*W*) increases with increasing number of cylinders as *W*=20*ND*. The computational domain is divided into 17398 quadrilateral linear finite elements for the two-cylinder system.

Figure 2 (a) shows the computational mesh around the two cylinders. Refined elements are used near the cylinder surface in order to capture the strong variations of the flow field. Each cylinder surface is divided into 96 finite elements and the minimum mesh size in the radius direction on the cylinder surface is 0.005*D*. The numerical results of VIV of the two-cylind er system are compared with those of 1DOF of vibration of a single circular cylinder system in the cross-flow direction.
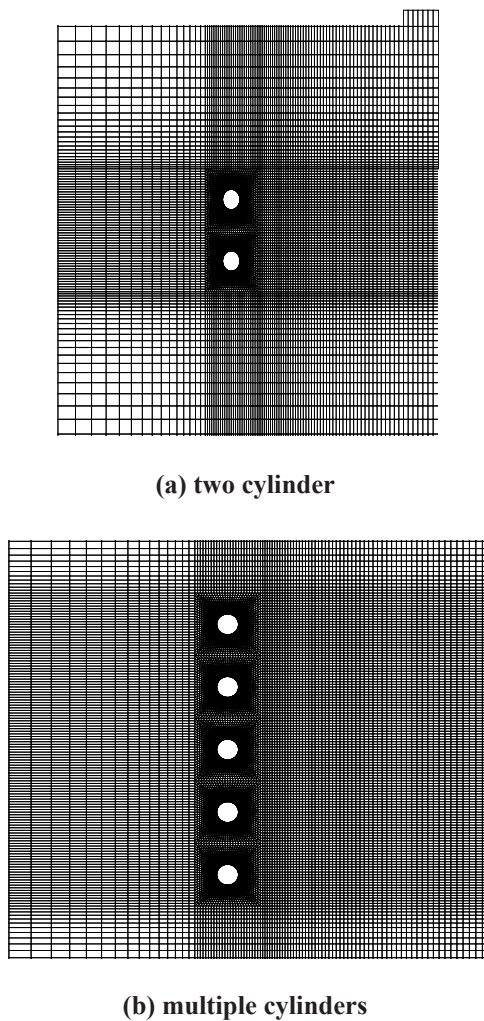

(a) two cylinder

(b) multiple cylinders

Figure 2. Computational mesh around the cylinders

Zhao [17] and Zhao et al. [38] compared the numerical results of VIV based on the same numerical model as used in this study with the published results in [13, 16, 29, 39] and obtained very good agreements. Zhao [17] validated the numerical model in the simulation of the VIV of two

tandem cylinders in fluid flow at Re=150. The validation of the numerical model on VIV simulation will not be repeated here. A mesh dependency study is carried out in order to ensure that the results are mesh-independent. Because the Reynolds number is kept to be a constant, the effects of the mesh density on the results are likely to be affected by the response amplitude. Additional simulations for the two-cylinder system at reduced velocities of 2, 4, 6, 8 and 10, where the response amplitudes are large, are carried out at a mesh denser than that shown in Figure 2.

The mesh shown in Figure 2 is referred to be the normal mesh. In the denser mesh, the circumference of each cylinder is divided into 128 elements and the minimum mesh size in the radial direction next to the cylinder surface is 0.002*D*. The total finite element node number of the denser mesh is 30,619. Table 1 shows the comparison between the results from the normal and denser meshes. For V_r=4 and 6, where the amplitude of the two cylinders are not the same (as shown in Figure 5), the maximum amplitude of the two cylinders is listed in Table 1. Both the amplitudes and the frequencies from the normal mesh agree well with those from the denser mesh. The difference in Table 1 is the percentage of the difference between the denser and normal mesh results. The maximum differences for the resultant vibration amplitude and the frequency are 1.7867% and 0.8114% respectively. The densities of the meshes for simulating the five- and ten-cylinder systems are the same as the normal mesh in the two-cylinder system.
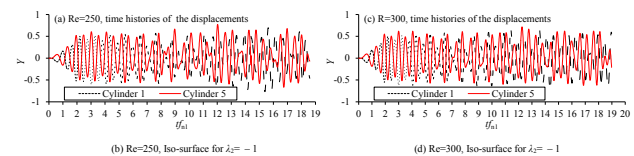

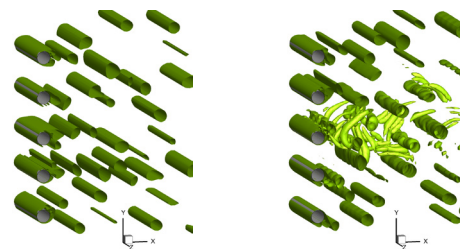**Figure 3.** Three-dimensional results of VIV of the five-cylinder system at V_r=7

Figure 4. shows the time histories of the displacements of the two cylinders at some typical reduced velocities for the two-cylinder system

The vibrations of the two cylinders are in anti-phase with each other when the reduced velocity $V_r \leq 2$ and

$V_r \geq 11$. At V_r=3 and 4, the vibrations of cylinders 1 and 2 are in phase with each other. At the reduced velocity of V_r=5 the vibrations of both cylinders contains two response modes and the vibrations of the two cylinders become in anti-phase with each other and the anti-phase sustains for all the reduced velocities greater than 5. It is interesting to see that the vibration amplitude of cylinder 1 is smaller than that of cylinder 2 at V_r=6. Regular beating responses of both cylinders are observed at V_r=6, especially in the response of cylinder 1. The beating period is approximately 10 times the cylinders' vibration period. It is believed that this is due to the asymmetry of vortex shedding at V_r=6, which will be discussed later on. The vibration responses of both cylinders at V_r=7 are almost perfectly regular and periodic. The same responses are observed for all $V_r \geq 7$ in the range of the reduced velocity covered in the present study.

Table 1. Comparison between the amplitudes and frequencies from the two meshes

V_r	Amplitude (A_y/D)			Frequency (f/f_{n1})		
	Denser mesh	Normal mesh	Difference (%)	Denser mesh	Normal mesh	Difference (%)
2	0.00980	0.00986	0.5618	0.4017	0.4050	0.8114
4	0.6341	0.6350	0.1543	0.9091	0.9043	0.5272
6	0.6239	0.6286	0.7493	1.4427	1.4327	0.6973
8	0.5325	0.5344	0.3462	1.6645	1.6654	0.0510
10	0.4458	0.4380	1.7867	1.8539	1.8492	0.2558

Figure 5 shows the variations of the amplitude, frequency and mean positions of the cylinders with the reduced velocity for the two-cylinder system. The high-amplitude reduced velocity range of the two-cylinder system is clearly wider than that of a single cylinder. The response amplitudes of the two- and single-cylinder systems follow a similar trend. The response amplitudes of the cylinders start to increase with increasing V_r at V_r=3 and reaches to the maximum values at about V_r=4. The response amplitudes of the two cylinders are different from each other at V_r=4 and 6. This is due to the asymmetry of the vortex shedding from the cylinders, which will be discussed in detail later on. The response amplitudes of the two cylinders become identical again as $V_r \geq 7$ and start to decrease rapidly as V_r increases from 7 to approximately 13. The response amplitudes decrease asymptotically at small rates from $V_r = 13$ towards a steady value of approximately 0.1 at $V_r = 30$. At V_r=4, the response frequency is close to the first-mode natural frequency and it increases to the second-mode natural frequency gradually as the reduced velocity is increased to 10.
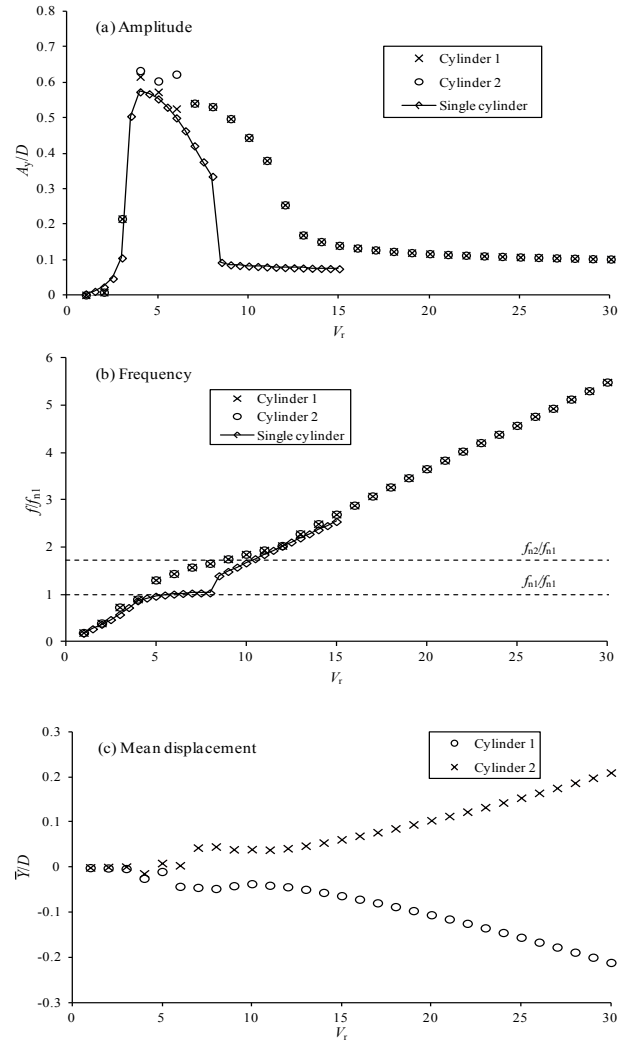

Figure 5. Variations of the amplitude, frequency and mean position of the cylinders with the reduced velocity for the two-cylinder system

Unlike a single cylinder where the lock-in between the vortex shedding frequency and the natural frequency in the regime of $4 \leq V_r \leq 8$ can be clearly identified based on the sudden changes in the response amplitude and frequency, the vibration frequencies of the two cylinders do not lock onto a fixed frequency in a reduced velocity range. For the two-cylinder system, the response frequency is between f_{n1} and f_{nN} when the reduced velocity is in the range of $3 \leq V_r \leq 10$. However, the response amplitude is still large when the response frequency is greater than the second mode natural frequency until the reduced velocity is 12. The amplitude of the two-cylinder system is reduced to a value less than 0.2 at V_r=13. The mean position of a cylinder in a multiple-cylinder system is defined as $\overline{Y}$. It can be seen in Figure 5 (c) that $\overline{Y}/D$ of both cylinders is very close to zero as $V_r \leq 5$. The mean position of cylinder 2 increases suddenly to about 0.05 at

$V_r = 7$. $\overline{Y}/D$ of the cylinder 2 decreases slightly with the increase of V_r between $7 \leq V_r \leq 12$ before it starts to increase with V_r. The mean position of cylinder 1 is approximately the mirror image of that of cylinder 2 about line of $\overline{Y}/D = 0$.

The response amplitudes of the cylinders are decomposed into different modes according to Eqs. (2) and (3) and the contribution of each mode is analyzed. Figure 6 shows the variation of the amplitude of the modal coordinates with the reduced velocity for the two-cylinder system. The amplitude of the n-th modal coordinate Y_n^* is defined as A_{yn}^*. It can be seen that the vibration is dominated by the first-mode when the reduced velocity is less than or equal to about 4 and by the second-mode when the reduced velocity exceeds or equal to about 6. Contributions from the two modes are comparable with each other between reduced velocity of 4 and 6 as shown in Figure 3 (d) and (e). For the two-cylinder system, the first- and second-mode shapes are $\{0.5642, 0.5642\}^T$ and $\{0.5642, -0.5642\}^T$, respectively. When the reduced velocity is greater than 7 the vibration contains only the second-mode, indicating that the vibration of cylinder 1 is always in anti-phase with that of cylinder 2.
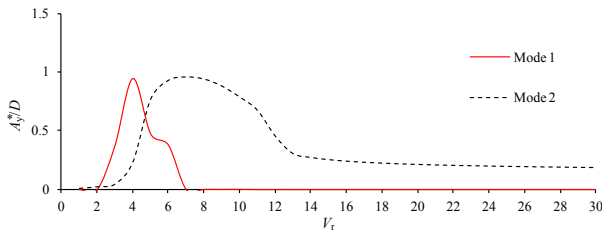

Figure 6. Variations of the amplitude of the generalized modal coordinates with the reduced velocity

Figure 7 shows the contours of nondimensional vorticity when cylinder 1 is at its lowest position for the two-cylinder system. The nondimensional vorticity ω is defined as $\omega = (\partial u_2 / \partial x_1 - \partial u_1 / \partial x_2)/(U/D)$. At $V_r = 3$ and 4, although the vibration displacements of the two cylinders are found to be in phase with each other as shown in Figure 4, the vortex shedding processes from the two cylinders are not exactly the same as each other as shown in Figure 7 (a) and (b). For example, the vortex shedding from cylinder 1 at $V_r = 3$ appears to lag the vortex shedding from cylinder 2. In Figure 7 (a), the positive vortex from cylinder 1 is shed from the cylinder after the positive vortex was shed from cylinder 2. In the wake, each negative vortex from cylinder 1 is shed earlier than that from cylinder 2 within one vortex shedding period. The phase difference between the vortex shedding flows from the two cylinders and the in-phase displacements lead to the phase difference between the vibration displacement and the lift

coefficient as shown in Figure 7 (b) and (c). At V_r=5 and 6, the vortex shedding from cylinder 1 differs from that from cylinder 2 significantly. The main characteristics of the vortex shedding flow at V_r=5 and 6 is that the wake from one cylinder is clearly wider than the one from the other. For example, the two-row vortex wake from cylinder 2 at V_r=6 is very similar to that at V_r=7, while that from cylinder 1 is clearly narrower than that of cylinder 2's wake. The vortex shedding flow at V_r=5 transits from the in-phase vibration mode to the anti-phase vibration mode. At V_r=7, the vortex shedding becomes symmetric with respect to y=0 line and the vibration displacements from the two cylinders are in anti-phase with each other. The symmetric flow patterns as shown in Figure 7 (e) and (f) are observed with the reduced velocity being greater than 7.
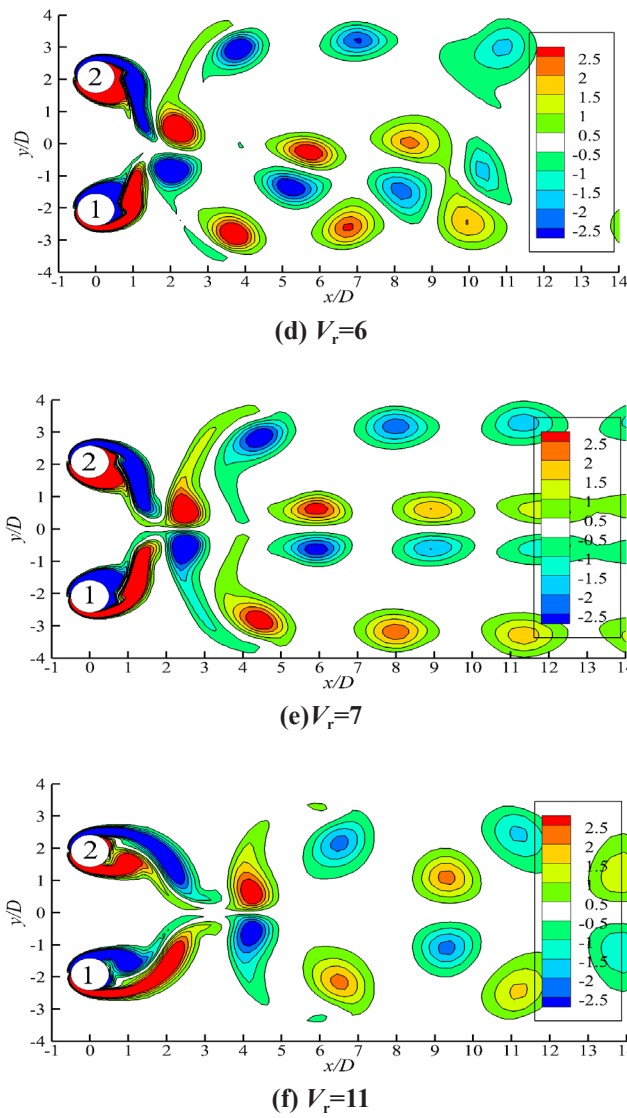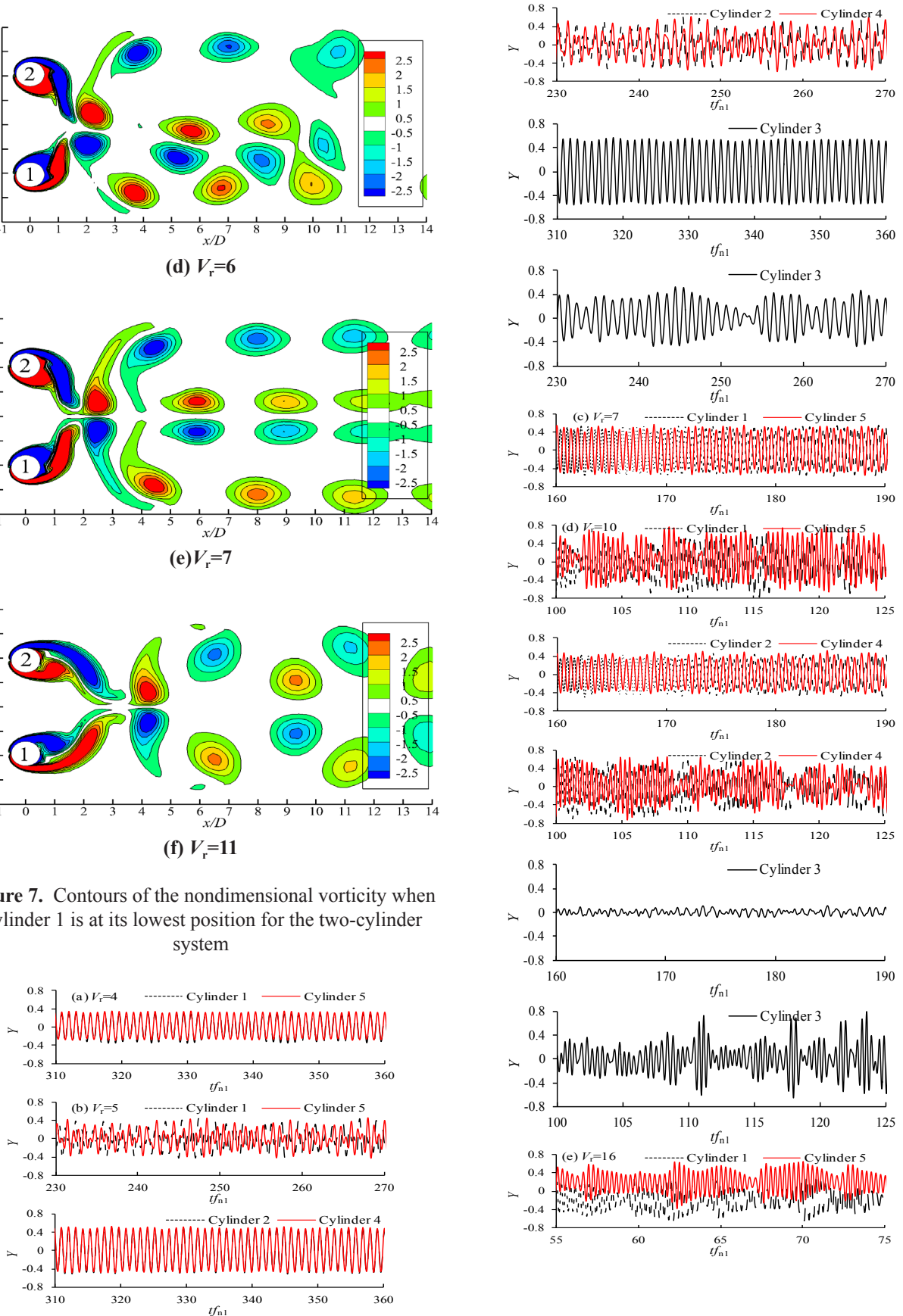

(a) V_r=3

(b)V_r=4

(c)V_r= 5

(d) V_r=6

(e) V_r=7

(f) V_r=11
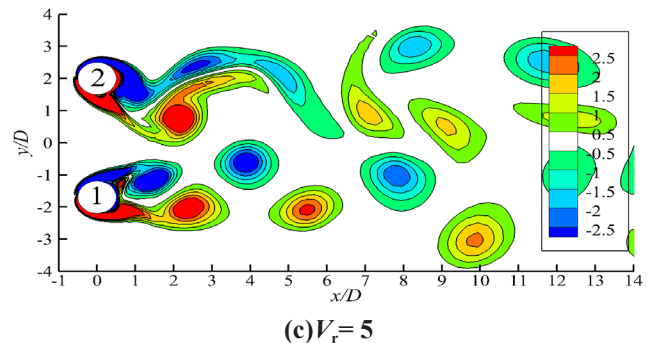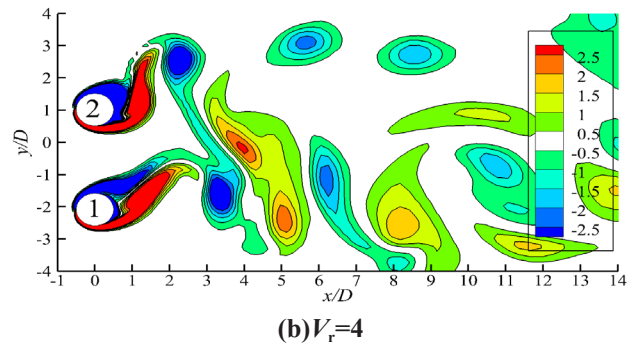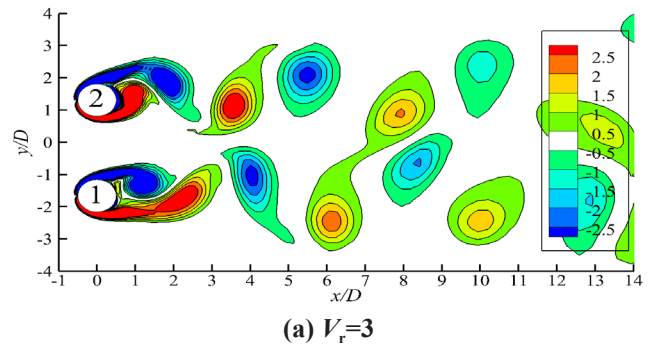
Figure 7. Contours of the nondimensional vorticity when Cylinder 1 is at its lowest position for the two-cylinder system
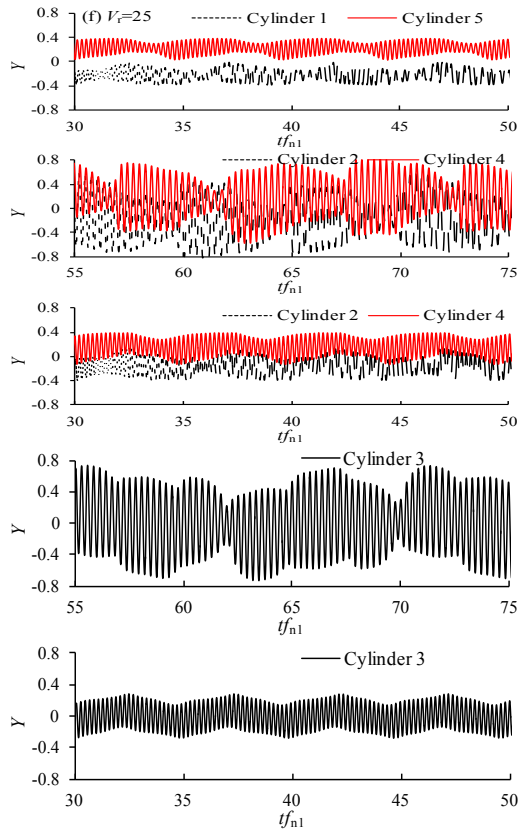
Figure 8. Time histories of the vibration displacement for the five-cylinder system

3.2 Five-cylinder System

The VIV of five elastically connected cylinders in a side-by-side arrangement is simulated in the reduced velocities range from 1 to 40 with an interval of 1. The computational mesh around the cylinders is shown in Figure 2 (b). Figure 8 shows the time histories of the responses of the five cylinders at some representative reduced velocities. The time histories of the responses of cylinders 1 and 5 are plotted together because they are geometrically symmetric about the central cylinder 3. The time histories of the responses of cylinders 2 and 4 are plotted together for the same reason. Similar to the two-cylinder system, the displacements of cylinders 1 and 2 are in phase with those of cylinders 5 and 3 respectively at V_r=3 and 4. The vibrations of all five cylinders become irregular at V_r=5. The vibration appears irregular due to the combination of more than one response modes in the response. The time histories of the responses of cylinders 1 and 2 are still generally in phase with those of cylinders 5 and 4 correspondingly at V_r=5. The vibration appears more irregular than that of the two-cylinder system because more frequency components are in the response. The frequencies of the irregular vibrations are analyzed using the Fast Fourier Transform (FFT).

Figure 9 shows the variations of the response amplitude, response frequency and the mean position of the cylinders with the reduced velocity for the five-cylinder system. For the cases with multiple-frequencies, Fast Fourier Transform is used to analyze the vibration and the frequency corresponding to the highest response amplitude in the FFT spectrum is the vibration frequency. The high-ampltude reduced velocity range for the five-cylinder system are much wider than that of a single cylinder and that of the two-cylinder system. The vibration amplitudes increase suddenly as the reduced velocity is increased to 4 and keep increasing until the reduced velocity is between 10 and 15, where the response amplitudes peak. The response amplitude and frequency of cylinders 1 and 2 are the same as those of cylinders 5 and 4 respectively except in the regime between 10 and 15. The first- to fifth-mode natural frequencies are marked in Figure 9 (b).
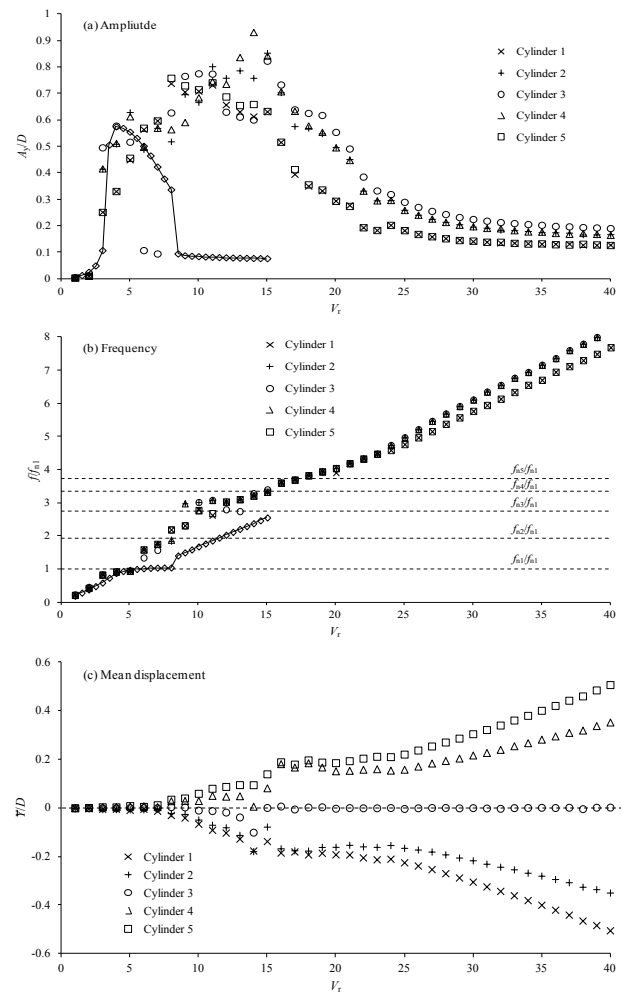

Figure 9. Variations of the response amplitude, response frequency and the mean position of the cylinder with the reduced velocity for the five-cylinder system

The response frequency exceeds f_{n5} as the reduced

velocity is greater than 18. After the response frequency exceeds f_{n5}, the response amplitudes of all five cylinders decrease gradually with increasing V_r. In the reduced velocity range of $3 \leq V_r \leq 18$ the response frequency is between the first- and fifth-mode frequencies. The upper boundary reduced velocity based on the highest natural frequency is V_{r5}=4.80. It is interesting to see that the response frequencies of the two side cylinders 1 and 5 are the same but they are slightly different from those of other middle cylinders 4 and 2. This is likely because of the difference between the approaching flow conditions to cylinders 1 and 2 (or cylinders 5 and 4), for example, caused by flow blockage and cylinder interference. The mean positions of the five cylinders remain to be around zero for $V_r \leq 7$ where response frequencies are closer to the first-mode natural frequency than other mode natural frequencies. The mean positions of cylinders 4 and 5 increases gradually to about 0.1 from V_r = 7 to V_r = 15 where the response frequencies of cylinders 4 and 5 increase from close to second-mode natural frequency to the fourth-mode natural frequency. There appear to be sudden increases of the mean positions of cylinders 4 and 5 from V_r = 15 to V_r = 16 which correspond to the changes of response frequencies from approximately 4th-mode natural frequency to 5th-mode natural frequency. The mean positions of cylinders 4 and 5 remain at steady values in the range of $16 \leq V_r \leq 25$ where response frequencies are greater than the 5th-mode natural frequency and the response amplitude reduces with increasing reduced velocity. The mean positions of cylinders 4 and 5 start to increase with V_r as V_r>25. The mean positions of cylinder 1 and cylinder 2 are approximately the mirror images of the mean positions of cylinders 5 and 4 about the line of $\overline{Y}/D = 0$.

Figure 10 shows the variations of the amplitude of the modal coordinates with the reduced velocity for the five-cylinder system. Mode 1 dominates the vibration response when the reduced velocity is less than 4 and mode 2 dominate the vibration when V_r=6 and 7. The vibration response is evenly dominated by Modes 1 and 2 at $V_r = 5$, which is the boundary reduced velocity between modes 1 and 2. As the reduced velocity exceeds 7, the contributions from modes 3 to 5 become significant while the modes 1 and 2 components of vibration response are still obvious. In the range of $8 \leq V_r \leq 15$, where the response energy is almost evenly distributed among the five modes, the amplitudes are obviously higher than those in other reduced velocities. The variation of the response frequency with the reduced velocity in the range of $8 \leq V_r \leq 15$ is also weak. The response is dominated by mode 5 as the reduced velocity exceeds 16. The response

frequency is close to the mode 5 frequency at V_r=16 and exceeds mode 5 frequency at V_r=17 as shown in Figure 9 (b). For the five-cylinder system the range $3 \leq V_r \leq 7$ is referred to be the single-mode branch because the single mode can be clearly identified except at the boundary between two modes. The range of $8 \leq V_r \leq 18$ is referred to be the multiple-mode branch. The reduced velocities of 16, 17 and 18 are in the multiple-mode branch because the contributions from modes 1 to 4 are obvious, but are less significant than that from mode 5.
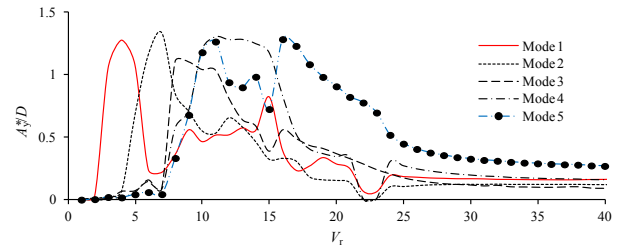

Figure 10. Variations of the amplitude of the modal coordinates with the reduced velocity for the five-cylinder system

Figure 11 shows vorticity contours of the near wakes of the cylinders when cylinder 1 is at its lowest position in the cross-flow direction. It can be seen that the interaction among the vortices are strong at V_r=4 to 16, where the response amplitudes of the cylinders are large. The interactions among the vortices shed from adjacent cylinders take place right behind the cylinders in Figure 11 (b) to (e). The strong interactions among the vortices lead to very irregular vibration displacement. Merging of the two or three vortices of the same signs is very common in the wake. It appears that the vortices that are shed from the bottom of cylinder 1 and the top of cylinder 5 are less affected by the interaction especially in Figure 11 (c).

(a) V_r=2

(b) V_r=4

(e) V_r=16

(c) V_r=7
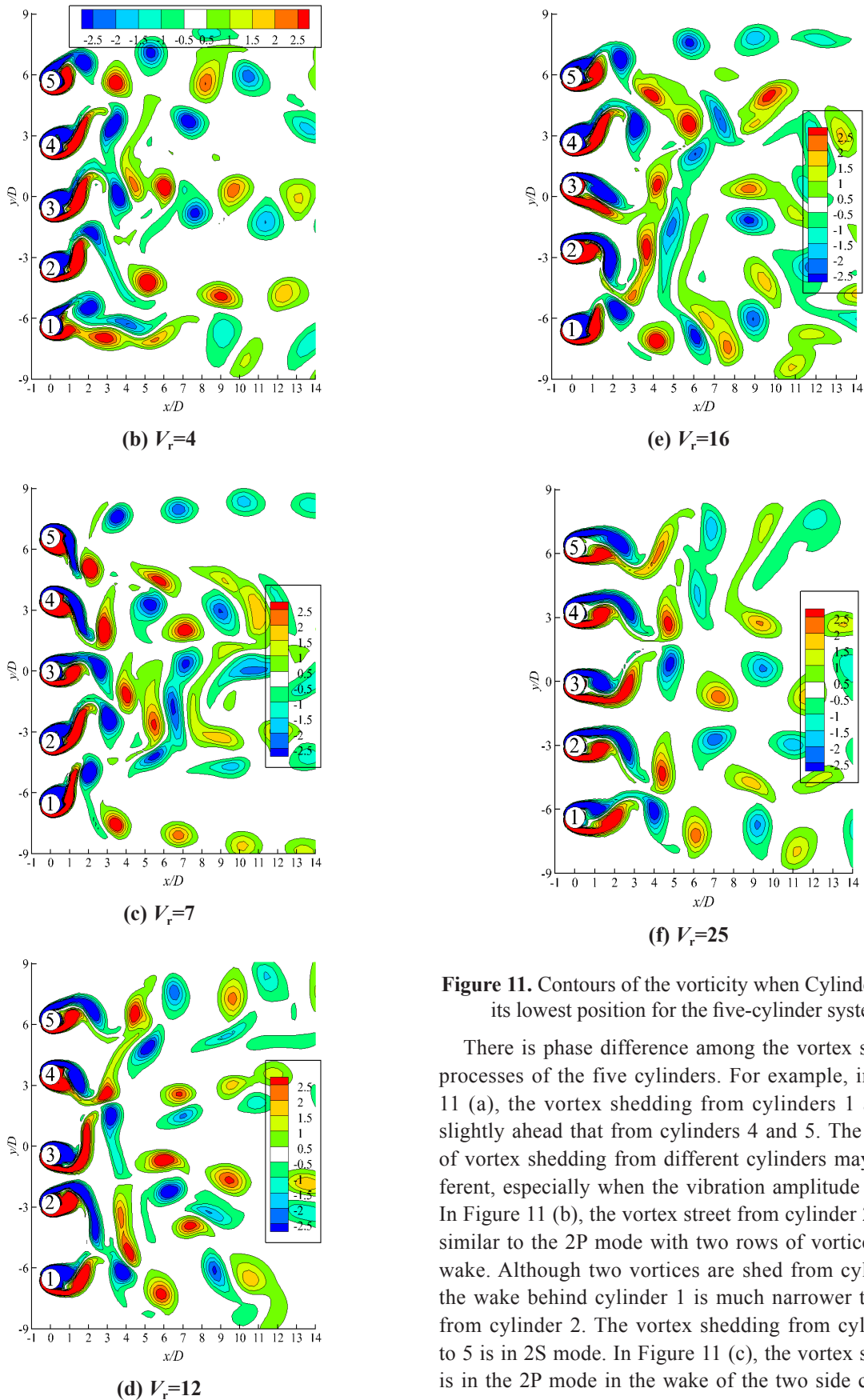

(f) V_r=25
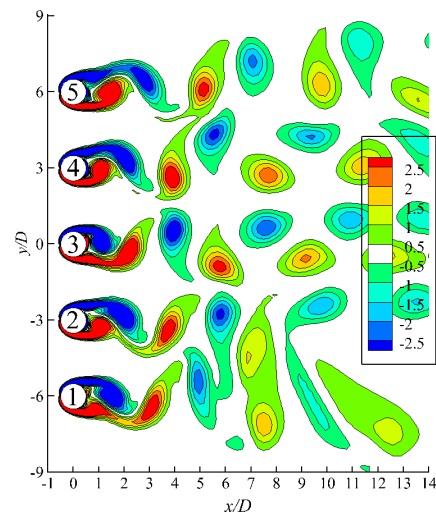
(d) V_r=12

Figure 11. Contours of the vorticity when Cylinder 1 is at its lowest position for the five-cylinder system

There is phase difference among the vortex shedding processes of the five cylinders. For example, in Figure 11 (a), the vortex shedding from cylinders 1 and 2 is slightly ahead that from cylinders 4 and 5. The patterns of vortex shedding from different cylinders may be different, especially when the vibration amplitude is large. In Figure 11 (b), the vortex street from cylinder 2 is very similar to the 2P mode with two rows of vortices in the wake. Although two vortices are shed from cylinder 1, the wake behind cylinder 1 is much narrower than that from cylinder 2. The vortex shedding from cylinders 3 to 5 is in 2S mode. In Figure 11 (c), the vortex shedding is in the 2P mode in the wake of the two side cylinders

DOI: https://doi.org/10.30564/hsme.v2i1.1504

1 and 5. The bottom row of the vortices from cylinder 1 and the top row of the vortices from cylinder 5 do not participate in the interactions with other vortices, while the vortices in the wake of the three middle cylinders interact actively.

3.3 Ten-cylinder System

Figure 12 shows the variation of the response amplitude, the response frequency and the mean positions with the reduced velocity for cylinders 1 to 5 in the ten-cylinder system. Figure 13 shows the variation of the amplitude of the modal coordinate with the reduced velocity for the ten-cylinder system. The cylinders are numbered from 1 to 10, with cylinder 1 at the bottom and cylinder 10 at the top. The statistic values of the response displacement for only five cylinders are shown in Figure 12 due to the symmetry of the configuration. Similar to those in the two- and five-cylinder systems, the cylinders do not vibrate until the reduced velocity exceeds 3. The amplitudes of all five cylinders increase quickly with the increasing reduced velocity as the reduced velocity is increased from 3 to 5. The differences among the amplitudes of the cylinders are significant. The response frequency of cylinder 1 exceeds f_{n10} at $V_r=37$ and those of cylinders 2 to 5 exceed f_{n10} at $V_r=31$. In the reduced velocity range of $3 \leq V_r \leq 31$, the frequencies of the majority cylinders (cylinders 2 to 9) are between f_{n1} and f_{n10}. Generally, the higher the reduced velocity, the higher mode of the response. Based on Figure 13, $3 \leq V_r \leq 15$ is the single mode branch, where single mode response can be clearly identified except at the boundaries between the two neighboring modes. $16 \leq V_r \leq 31$ is the multiple-mode branch where multiple modes co-exist. The response in the range of $16 \leq V_r \leq 23$ contains almost all the modes and that in the range of $24 \leq V_r \leq 31$ is dominated by even modes 2, 4, 6, 8 and 10. The increasing rate of the response frequency with the reduced velocity in the multiple-mode branch $24 \leq V_r \leq 31$ is smaller than that in other ranges of reduced velocity. The response amplitude in the range of $16 \leq V_r \leq 23$ is higher than those in other ranges. In the regime of $16 \leq V_r \leq 23$, the maximum amplitudes of cylinders 1 to 5 range from 0.6 to 1.
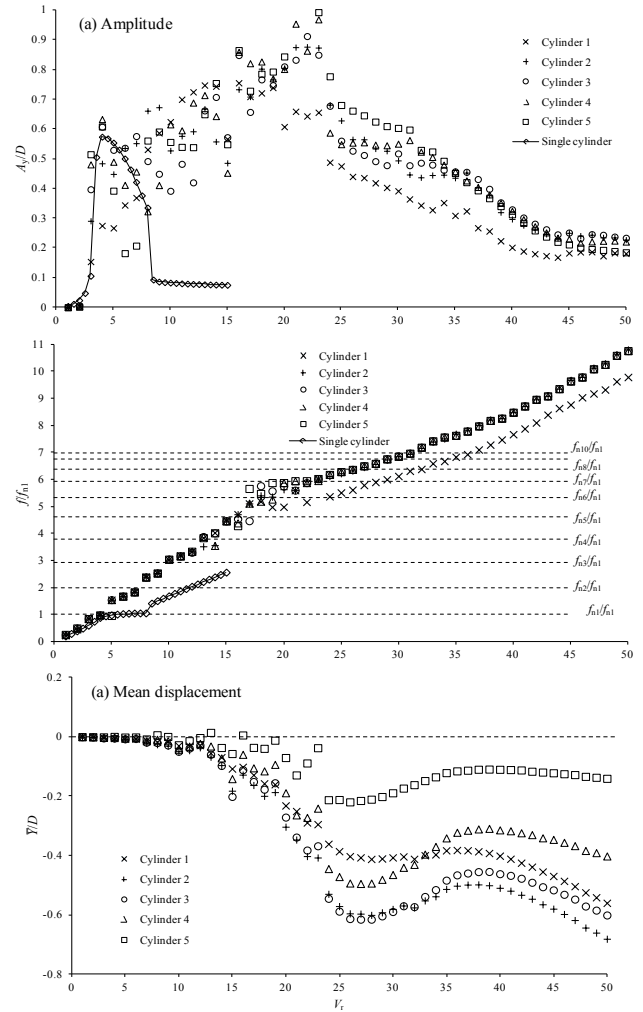

Figure 12. Variation of the response amplitude, the response frequency and the mean displacement with the reduced velocity for the five cylinders in the ten-cylinder system

In the single-mode branch of $3 \leq V_r \leq 15$, the response of the cylinder system is mainly dominated by one mode or two modes at the boundary reduced velocity between two modes. In Figure 13, the response is predominated by modes 1, 2, 3, 4 and 5 at $V_r=3, 7, 9, 11, 13$, respectively. The reduced velocities of 5, 8, 10 and 12 are the boundaries between two adjacent modes. The amplitude of cylinder 1 becomes the smallest among others once the reduced velocity exceeds 20. After the reduced velocity exceeds 23, the response amplitudes of all the five cylinders decrease with the increasing V_r until $V_r=45$, after which the response amplitudes are small and changes little. It is interesting to see that, starting from $V_r=20$, the response frequency of cylinder 1 starts being lower than those of other four cylinders till the largest reduced velocity simulated. The variation of the mean positions of the

cylinders with the reduced velocity for the ten-cylinder system is similar to those for the two- and five-cylinder systems. The non-dimensional mean displacements of cylinders 1 to 5 reaches its maximum at about $V_r = 26$ and then starts decreasing with the increasing V_r until V_r is about 38.

As the reduced velocity is greater than 15, the response frequency is greater than the fifth-mode frequency f_{n5}, however, the components of the modes 1 to 5 are still obvious as shown in Figure 13 (a) and there is no obvious difference between them and those of modes 6 to 10. Modes 6 to 10 appear to contribute to the response evenly based on Figure 13 (b) and their contributions on the amplitude are generally about 50% greater than those from Modes 1 to 5. The reason why different modes contribute to the response displacement evenly at large reduced velocities is the closeness among the modal frequencies. It can be seen in Figure 12 (b) that the modal frequencies for Modes 6 to 10 are very close to each other and the vibration can shift from one mode to another due to a very small disturbance. The strong interaction among the wakes from the cylinders provides the disturbance easily, especially when the amplitudes of the vibration are high. When the reduced velocity is greater than 25, the contribution from odd number modes are negligibly smaller than those from the even number modes, indicating that the vibration displacement is anti-symmetric with respect to the line of symmetry $y=0$. The response is dominated by the highest mode (Mode 10) as the reduced velocity exceeds 32.
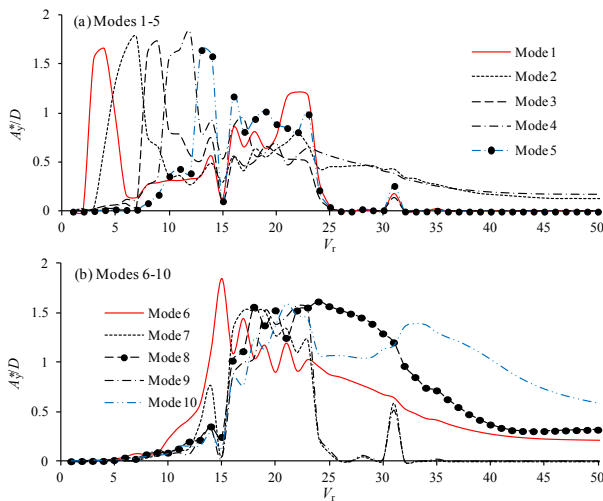

Figure 13. Variations of the amplitude of the generalized modal coordinates with the reduced velocity for the ten-cylinder system

3.4 Comparison between the Systems

The range of the reduced velocity for lock-in is of interest in many engineering applications. To compare the lock-in range of all the response modes. The reduced velocity defined based on the natural frequency of the *n*-th mode (f_{nn}) can be calculated by $U/(f_{nn}D)$ and is defined as the n-th modal reduced velocity. The variations of the amplitude of the modal coordinate with the modal reduced velocity for the two-, five- and ten-cylinder systems are shown in Figure 14. It can be seen that, if the reduced velocity is normalized based on f_{nn}, the lock-in range of different modal amplitudes are very close to each other. For all the response modes, the lock-in starts from $U/(f_{nn}D) \approx 2$ and ends at a reduced velocity in a small range of $6 \leq U/(f_{nn}D) \leq 8$. Based on this conclusion, it is possible to estimate the dimensional lock-in velocity for every response mode. For a single cylinder, the lock-in range reduced velocity is $2 \leq U/(f_n D) \leq 8$. It can be seen that the upperboundaries of the lock-in range of the modal reduced velocity for some modes are slightly smaller than that of a single cylinder.

Although different modes have different lock-in range of the modal reduced velocity. Because the dimensional velocity ranges for lock-in of different modes overlap with each other, the high-amplitude vibration of the cylinder occurs in a wide range of velocity for multiple cylinder systems, and the dimensional high-amplitude response range of the velocity increases with increasing cylinder number. If we use $2 \leq U/(f_{nn}D) \leq 8$ as the lock-in range of the modal reduced velocity, the lower and upper boundaries of the global dimensional lock-in velocity range (the total high-amplitude response range of the velocity) can be approximately estimated to be the lower boundry of the first mode and the higher boundary of the highest mode, respectively.

4. Conclusions

Vortex-induced vibration (VIV) of multiple elastically connected side-by-side circular cylinders in steady flow at a low Reynolds number of 150 is investigated numerically. The cylinders are allowed to vibrate only in the cross-flow direction. The Navier-Stokes equations and the equation of motion are solved numerically for simulating the flow and vibration of the cylinders, respectively.

Unlike the single cylinder case, distinct lock-in a range of the reduced velocity where the response frequency remains almost constant is not observed. Instead, the response frequency increases continuously with the increase in the reduced velocity in the multiple-cylinder system. High amplitude vibration is found when the response frequency is between the lowest and the highest natural frequencies. After the response frequency exceeds the highest natural frequency, the response amplitude reduces

with increasing reduced velocity, but remains high for a small range of reduced velocities.

The modal coordinates of the response are analyzed in order to understand the contribution of each mode in the response. It is found that the response is generally in high mode at high reduced velocities for the five- and ten-cylinder systems. The dominance of a single mode in the vibration can only be found for low modal frequencies. The single-mode response can be found in the range of $3 \leq V_r \leq 7$ for the five cylinder system and $3 \leq V_r \leq 15$ for the ten cylinder system. At higher reduced velocities the contributions of all the response modal shapes are found to be comparable with each other. This is because the closeness among the high modal frequencies makes the vibration switching from one mode to another easily under even very small disturbances, while the strong interaction among the wake flows provides the source of disturbances. Based on the results for the five- and ten-cylinder systems, it is found that the single mode for about half of the natural frequencies can be identified, while the lowest frequency has the clearest single mode.

In the two-cylinder system, the response amplitudes of the two cylinders are the same except in the range of $4 \leq V_r \leq 6$, where the response amplitudes reach to their maximum values. For the five- and ten-cylinder systems, the response amplitudes of the cylinders are not the same and the difference among the amplitudes of the cylinders is high when the response amplitude is high. Strong interactions among the vortex shedding flows from different cylinders occur at high response amplitudes, resulting in a chaotic vortex shedding pattern. There are large phase differences among the vortex shedding processes from different cylinders in a multiple-cylinder system.

References

[1] Williamson, C. H. K. and Roshko, A.. Vortex formation in the wake of an oscillating cylinder. Journal of Fluids and Structures, 1988, 2: 355-381.

[2] Sarpkaya, T.. A critical review of the intrinsic nature of vortex-induced vibrations. Journal of Fluids and Structures, 2004, 19: 389–447.

[3] Govardhan, R., Williamson, C. H. K.. Modes of vortex formation and frequency response for a freely-vibrating cylinder. Journal of Fluid Mechanics, 2000, 420: 85-130.

[4] Williamson, C.H.K., Govardhan, R.. Vortex-induced vibrations. Annual Review of Fluid Mechanics, 2004, 36: 413–455.

[5] Sarpakaya, T., Isaacson, M.. Mechanics of wave forces on offshore structures (first ed). Van Nostrand Reinhold, 1981.

[6] Khalak, A., Williamson, C.H.K.. Dynamics of a hydroelastic cylinder with very low mass and damping. Journal of Fluids and Structures, 1996, 10: 455–472.

[7] Khalak, A., Williamson, C. H. K.. Motions, forces and mode transitions in vortex-induced vibrations at low mass-damping, Journal of fluids and Structures, 1999, 13: 813-851.

[8] Jauvtis, N., Williamson, C. H. K.. The effect of two degrees of freedom on vortex-induced vibration at low mass and damping, Journal of Fluid Mechanics, 2004, 509: 23-62.

[9] Fredsøe, J., Sumer, B.M., Andersen, J., Hansen, E.A.. Transverse vibration of a cylinder very close to a plane wall. In: Proceedings of the Fourth International Symposium on Offshore Mechanics and Arctic Engineering. Dallas, ASME, 1985, 1: 601-609.

[10] Gao, F.P., Yang, B., Wu, Y.X., Yan, S.M.. Steady currents induced seabed scour around a vibrating pipeline. Applied Ocean Research, 2006, 26: 291–298.

[11] Yang, B., Gao, F.P., Jeng, D.S., Wu, Y.X.. Experimental study of vortex-induced vibrations of a pipeline near an erodible sandy seabed. Ocean Engineering, 2008, 35: 301–309.

[12] Zhao, M., Cheng, L.. Numerical simulation of two-degree-of-freedom vortex induced vibration of a circular cylinder close to a plane boundary. Journal Fluids and Structures, 2011, 27: 1097-1110

[13] Singh, S.P, Mittal, S.. Vortex-induced oscillations at low Reynolds numbers: Hysteresis and vortex-shedding modes. Journal of Fluids and Structures, 2005, 20: 1085–1104.

[14] Leontini, J.S., Stewart, B.E., Thompson, M.C., Hourigan, K.. Wake-state and energy transitions of an oscillating cylinder at low Reynolds number. Physics of Fluids, 2006, 18: 067101.

[15] Mittal, S., Kumar, Y.. Finite element study of vortex-induced cross-flow and in-line oscillations of a circular cylinder at low Reynolds numbers. International Journal for Numerical Methods in Fluids, 1999, 31: 1087-1120.

[16] Bao, Y., Zhou, D., Tu, J.. Flow interference between a stationary cylinder and an elastically mounted cylinder arranged in proximity. Journal of Fluids and Structures, 2011, 27: 1425–1446.

[17] Zhao, M.. Flow induced vibration of two rigidly coupled circular cylinders in tandem and side-by-side arrangements at a low Reynolds number of 150. Physics of Fluids, 2013, 25: 123601.

[18] Pan, Z.Y., Cui, W.C., Miao, Q.M.. Numerical simulation of vortex-induced vibration of a circular cylinder at low mass-damping using RANS code. Journal of Fluids and Structures, 2007, 23: 23-37.

[19] Guilmineau, E., Queutey, P.. Numerical simulation of vortex-induced vibration of a circular cylinder with low mass damping in a turbulent flow. Journal of Fluids and Structures, 2004, 19: 449-466.

[20] Kim, H. J., Durbin, P. A.. Investigation of the flow between a pair of circular cylinders in the flopping regime. Journal of Fluid Mechanics, 1988, 196: 431-448.

[21] Alam, M. M., Moriya, M., Sakamoto, H.. Aerodynamic characteristics of two side-by-side circular cylinders and application of wavelet analysis on the switching phenomenon. Journal of Fluids and Structures, 2003, 18: 325-346.

[22] Afgan, I., Kahil, Y., Benhamadouche, S., Sagaut, P.. Large eddy simulation of the flow around single and two side-by-side cylinders at subcritical Reynolds numbers. Physics of Fluids, 2011, 23: 075101.

[23] Thapa, J., Zhao, M., Cheng, L., Zhou, T.. Three-dimensional simulations of flow past two circular cylinders in side- by-side arrangements at right and oblique attacks. Journal of Fluids and Structures, accepted on Feburay 10, 2015.

[24] Huera-Huarte, F.J., Gharib, M.. Flow-induced vibrations of a side-by-side arrangement of two flexible circular cylinders. Journal of Fluids and Structures, 2011, 27: 354–366.

[25] Wang, X.Q., So, R.M.C., Xie, W.-C, Zhu, J.. Free-stream turbulence effects on vortex-induced vibration of two side-by-side elastic cylinders. Journal of Fluids and Structures, 2008, 24: 664-679.

[26] Assi, G.R.S., Meneghini, J.R., Aranha, J.A.P., Bearman, P.W., Casaprima, E.. Experimental investigation of flow-induced vibration interaference between two circular cylinders. Journal of Fluids and Structures, 2006, 22: 819-827.

[27] Kim, S., Alam, M.M., Sakamoto, H., Zhou, Y.. Flow-induced vibrations of two circular cylinders in tandem arrangement. Part 1: Characteristics of vibration. Journal of Wind Engineering and Industrial Aerodynamics, 2009, 97: 304-311.

[28] Mittal. S., Kumar, V.. Flow-induced oscillations of two cylinders in tandem and staggered arrangements. Journal of Fluids and Structures, 2001, 15: 717-736.

[29] Borazjani, I, Sotiropoulos, F.. Vortex-induced vibrations of two cylinders in tandem arrangement in the proximity-wake interference region. Journal of Fluid Mechanics, 2009, 621: 321-364.

[30] Carmo, B.S., Assi, G.R.S., Meneghini, R.. Computational simulation of the flow-induced vibration of a circular subjected to wake interference. Journal of Fluids and Structures, 2013, 41: 99–108.

[31] Jester,W., Kallinderis, Y.. Numerical study of incompressible flow about transversely oscillating cylinder pairs. Journal of Offshore Mechanics and Arctic Engineering-Transactions of the ASME, 2004, 126: 310-317.

[32] Duarte, F., Gormax, R., Natesan, S.. Arbitrary Largrangian-Eulerian method for Navier-Stokes equations with moving boundaries. Comput. Methods Appl. Mech. Engrg., 2004, 193: 4819-4836.

[33] Nobari, M.R.H., Ghazanfarian, J.. A numerical investigation of fluid flow over a rotating cylinder with cross flow oscillation. Computers & Fluids, 2009, 38: 2026-2036.

[34] Sumner, D.. Two circular cylinders in cross-flow: A review. Journal of Fluids and Structures, 2010, 26: 849-899.

[35] Zhao, M., Cheng, L., An, H., Lu, L.. Three-dimensional numerical simulation of vortex-induced vibration of an elastically mounted rigid circular cylinder in steady current. Journal of Fluids and Structures, 2014, 50: 292-311.

[36] Jeong, J., Hussain, F.. On the identification of a vortex. Journal of Fluid Mechanics, 1995, 285: 69-94.

[37] Papaioannou, G.V., Yue, D.K.P.. Triantafyllou, M.S., Kariadakis, G.E.. Three-dimensionality effects in flow around two tandem cylinders. Journal of Fluid Mechanics, 2006, 558: 387-413.

[38] Zhao, M., Cheng, L., Zhou, T.. Numerical simulation of vortex-induced vibration of a square cylinder at a low Reynolds number. Physics of Fluids, 2013, 25: 023603.

[39] Ahn, H.T., Kallinderis, Y.. Strongly coupled flow/structure interactions with a geometrically conservative ALE scheme on general hybrid meshes. Journal of Computational Physics, 2006, 219: 671–696.